Hindawi
Journal of Nanomaterials
Volume 2019, Article ID 6042026, 9 pages
https://doi.org/10.1155/2019/6042026

Research Article

Graphene Quantum Dots-Modified Ternary ZnCdS Semiconductor for Enhancing Photoelectric Properties

Zicong Jiang,[1] **Yun Lei**,[1] **Mingzhen Zhang**,[2] **Zheng Zhang**,[1] **and Zhong Ouyang**[1]

[1]*School of Resources and Environmental Engineering, Wuhan University of Technology, Wuhan 430070, China*
[2]*Hubei Entry & Exit Inspection and Quarantine Bureau Technology Center, Wuhan 430050, China*

Correspondence should be addressed to Yun Lei; leiyun@whut.edu.cn

Received 14 March 2019; Revised 22 April 2019; Accepted 13 May 2019; Published 9 June 2019

Academic Editor: Haisheng Qian

A series of graphene quantum dots-modified ZnCdS (ZnCdS/G) composites with different contents of graphene quantum dots (GQDs) were prepared by a solvothermal route and characterized via various measurements. GQDs have a type graphene height of 2 nm and exhibit an excitation-dependent PL behavior. GQDs-modified ZnCdS composites present good lattice fingers that can be assigned to the (110) plane of GQDs and (112) plane of ZnCdS. The effect of different GQDs contents on the photoelectric property of ZnCdS was investigated. The results show that the photocurrent density of ZnCdS/G first increases and achieves a maximum of 11.4 $\mu A/cm^2$ with the addition of 0.06 wt% and then decreases as the GQDs content changes from 0.06 wt% to 0.12 wt%. Photocurrent counts as a function of time present a decrease of 10% and remains stable after 1600 s.

1. Introduction

In the past, semiconductor materials have captured much attention on environmental cleaning, solar energy utilization, photovoltaic devices, and diode devices due to their great photoelectric properties [1–8]. Among them, II–VI semiconductors, such as ZnS and CdS, have been extensively studied for their proper bandgap and sensitive photoelectric reaction [9–11]. However, the individual ZnS or CdS semiconductor is restricted by its fast recombination rate of photogenerated electron-hole pairs, relatively wide bandgap energy, and photocorrosion reaction [12–15]. In order to conquer these difficulties, ternary semiconductor and carbon modification materials were proposed. Compared to the individual ZnS or CdS semiconductor, the heterostructures display a tunable bandgap which can achieve a significant improvement in the generation, transmission, and lifetime of charge carriers [16, 17]. Therefore, many researches have explored the ternary ZnCdS semiconductor. Recently, Chen et al. prepared $Zn_xCd_{1-x}S$ NC nanocrystals to investigate the effect of surface structure on the band edge emission and further drew a conclusion that the surface ligands of the $Zn_{0.8}Cd_{0.2}S$ affect the optical properties and quantum yields [18, 19]. Chen et al. fabricated hollow ZnCdS dodecahedral cages with outstanding photoelectric properties for efficient H_2 evolution [20]. Zhang et al. successfully enhanced the photoelectric property of $Zn_xCd_{1-x}S$ nanorods via adjusting the composition of the composite [21]. Although these results have demonstrated that a ternary semiconductor provides a promising potential for improving the photoelectric property, there is still plenty of room in exploring novel carbon-based materials for the high performance of a ternary semiconductor.

Graphene quantum dots (GQDs), a kind of novel carbon material, are small graphene sheets with the lateral size of less than 100 nm in single- or few-layer graphene [22, 23]. GQDs exhibited unique photoelectronic properties, including the tunable bandgap, unique upconverted photoluminescence behavior, excellent optical stability, and strong visible light absorption due to the quantum confinement and strong edge effects [24–29]. The excellent conductivity and abundant active sites on the surface of GQDs make it an ideal and multifunctional platform for integrating with diverse semiconductor materials [30–32]. Chen et al. developed GQDs-decorated ZnS nanobelts for efficient environmental cleaning via a facile hydrothermal process [18]. Tian et al.

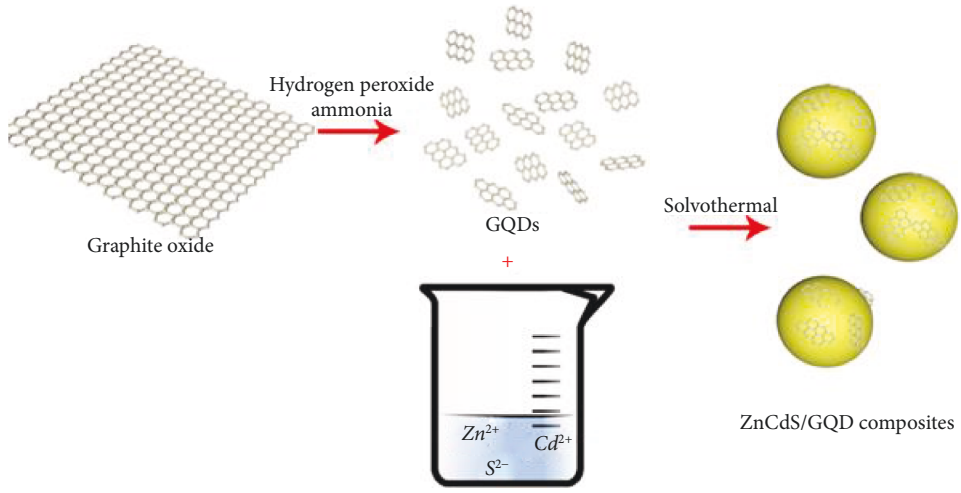

Scheme 1: Schematic diagram of the synthesis of ZnCdS/G composites.

prepared the N, S-GQDs-rGO-TiO_2 nanotube composites with superior material properties for efficient photocatalytic degradation [33]. Lei et al. developed strongly coupled CdS/GQDs nanomaterials with remarkable photocatalytic hydrogen evolution reactions under the irradiation of visible light [34]. These results suggest that GQDs play an important role in improving the performances of semiconductor materials. Therefore, a GQDs-modified semiconductor seems to be a good way to change the photoelectric properties of the semiconductor. Based on our previous work [35, 36], the combination of GQDs and ZnCdS was further investigated as no related work has yet been reported. Meanwhile, the effect of GQDs on the photoelectric performance of GQDs-modified ZnCdS composites was investigated by a series of contrast experiments.

Herein, ZnCdS/G composites with different contents of GQDs were synthesized in which GQDs were prepared by a simple cutting from graphite oxide. Atomic force microscopy, UV-visible spectra, photoluminescence spectra, zeta potential, XRD, HRTEM, and X-ray photoelectron spectroscopy were employed to identify the morphology, structure, surface state, and crystal phase of the prepared samples. The photoelectric properties of ZnCdS modified with different GQDs contents were investigated by the photocurrent-time responses and electrochemical impedance spectra.

2. Experimental

2.1. Materials. Graphite powder (chemical purity (CP), 99.85%), ammonia (NH_3, 25%), hydrogen peroxide (H_2O_2, 30%), sulfuric acid (H_2SO_4, 98%), sodium nitrate ($NaNO_3$), potassium permanganate ($KMnO_4$), zinc acetate ($C_4H_6O_4Zn{\cdot}2H_2O$), cadmium acetate ($C_4H_6CdO_4{\cdot}2H_2O$), thiourea (H_2NCSNH_2), ethylene glycol ($HOCH_2CH_2OH$), and ethanol (CH_3CH_2OH) were commercially available products.

2.2. Preparation of GQDs. Graphite oxide (GO, 540 mg) prepared by the modified Hummers method was dispersed into mixtures of 10 ml ammonia and 40 ml hydrogen peroxide. The mixtures were loaded into a Teflon-lined stainless steel autoclave and heated at 180°C for 12 h. The cooling reaction products were centrifuged at 8000 rpm for 10 minutes, and the suspension was filtered with a 0.22 μm filter. The final solution was graphene quantum dots.

2.3. Preparation of ZnCdS/G Composites. The experiments of ZnCdS/G composites were operated in the one-step solvothermal method illustrated by Scheme 1. Briefly, 2.5 mmol cadmium acetate, 2.5 mmol zinc acetate, and 5 mmol thiourea were dissolved in 80 ml ethylene glycol. After that, different contents of GQDs were added to the solutions and sonicated for 30 minutes. In the end, the solutions were loaded into the autoclaves of 100 ml capacity and heated at 140°C for 4 hours. The cooled products were repeatedly washed with ethanol and dried in an oven at 50°C. The ZnCdS/G composites with 0.03 wt%, 0.06 wt%, and 0.12 wt% GQDs were named as ZnCdS/G-0.03, ZnCdS/G-0.06, and ZnCdS/G-0.12, respectively. The pure ZnCdS was prepared by the same procedures without adding the GQDs. To prepare the working electrode, 50 mg composites and 100 mg polyethylene glycol were mixed and grinded with 1 ml ethanol to make a slurry. The slurry was coated onto a clean FTO glass by the doctor blade method. The films on FTO were annealed at 400°C for 30 min to remove the polyethylene glycol in N_2 flow.

2.4. Characterization. Atomic force microscopy (AFM) images were collected by a Bruker MultiMode 8 in the PeakForce Tapping mode of the mica substrate using 2 nm silicon nitride probes. The structural information was characterized by X-ray diffraction (XRD, X'Pert3 Powder) using Cu Kα radiation (λ = 1.5406 Å), and the morphological images were observed on a high-resolution transmission electron microscope (HRTEM, JEOL, JEM2100F). X-ray photoelectron spectroscopy (XPS) analysis was conducted using a Thermo ESCALAB 250Xi device. The UV-visible spectra were carried out on a UV-5500 spectrophotometer with the wavelength from 190 to 800 nm. Photoluminescence (PL) spectra were recorded on a Cary Eclipse fluorescence spectrophotometer.

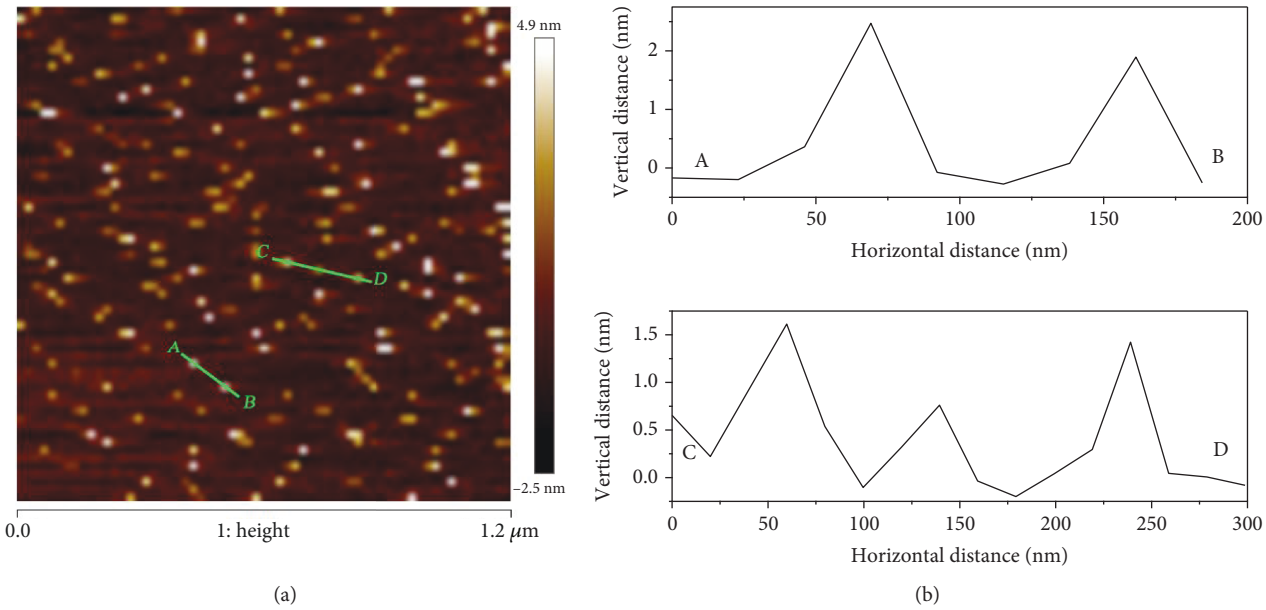

Figure 1: AFM images of GQDs.

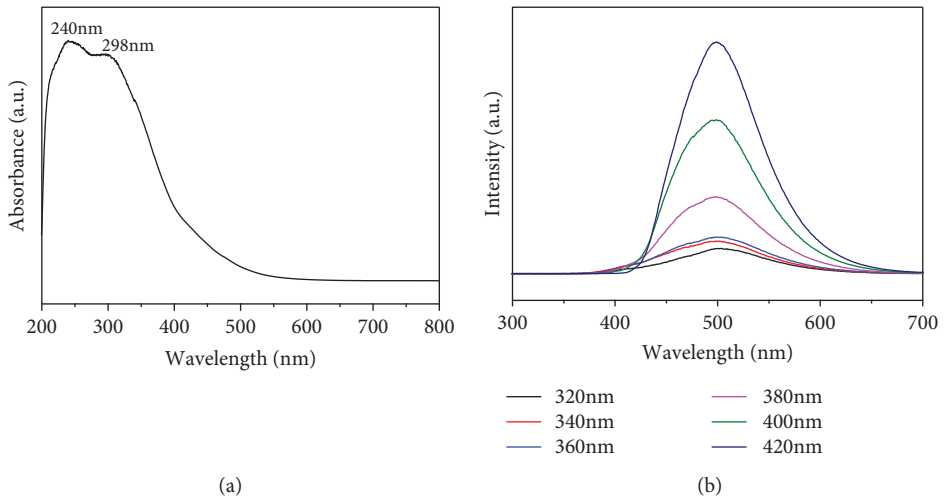

Figure 2: UV-visible (a) and PL (b) spectra of GQDs.

Zeta potential was detected by a Brookhaven BI-90 Plus Particle Size Analyzer. Photocurrent-time response as well as the electrochemical impedance spectroscopy measurements was performed on an electrochemical work station (CHI650e) in a three-electrode system. As FTO glass coated with samples was served as the working electrode, a standard calomel electrode and a platinum foil were applied as the reference electrode and the counter electrode, respectively.

3. Results and Discussion

The morphology of the GQDs was observed on AFM, and the result is shown in Figure 1. GQDs are evenly dispersed with the lateral size of 50 nm and thickness of 2 nm. UV-visible absorption spectra and PL spectra were used to evaluate optical properties of GQDs as shown in Figure 2. For the UV-visible spectra, there is a strong peak at 240 nm derived from the π-π^* transition of the C=C bond and a weak one signal ascribed to the n-π^* transition of the C=O bond that suggest the presence of carboxyl groups on the surface of GQDs [37]. In the PL spectra of GQDs, the PL intensity orderly increases as the excitation wavelength increases from 320 nm to 420 nm, exhibiting an excitation-dependent PL behavior. The PL peaks around 501 nm show a green emission due to the efficient edge groups of carboxyl, which is consistent with the result of UV-visible absorption spectra of GQDs [38]. There is nonshifting of the GQDs attributed to the high-oxidation degrees of the surface oxidation [39].

The zeta potential was tested to analyze the surface charge of GQDs, ZnCdS, and ZnCdS/G-0.06 in an aqueous solution of pH 7. The results are presented in a histogram as shown in Figure 3. GQDs exhibit a negative zeta potential

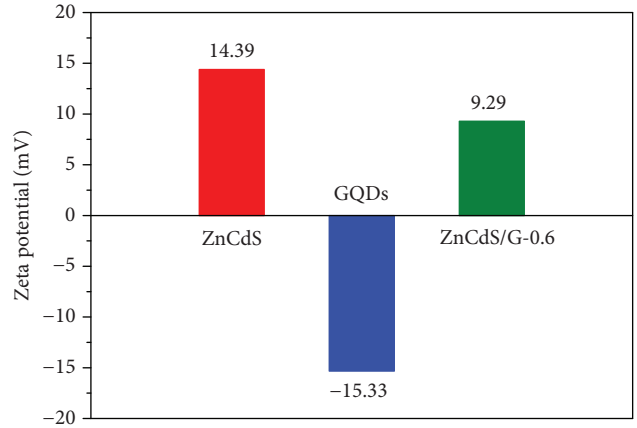

Figure 3: Zeta potential of GQDs, ZnCdS, and ZnCdS/G-0.06 under the condition of pH 7.

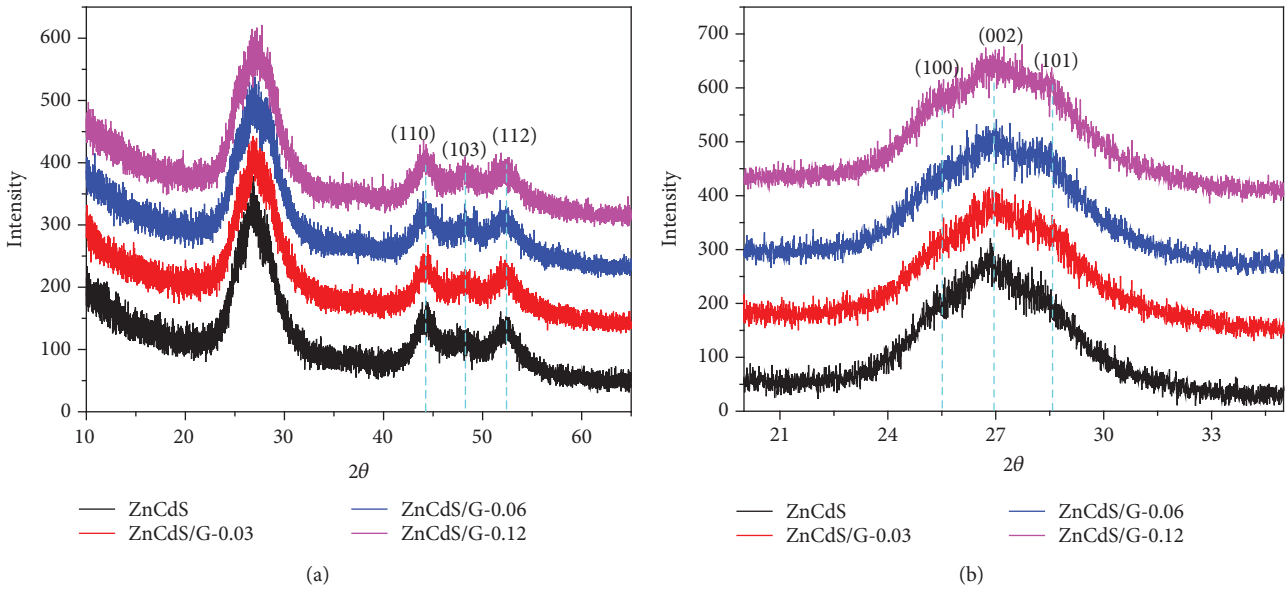

Figure 4: XRD patterns of pure ZnCdS and ZnCdS/G composites with different amounts of GQDS: (a) XRD patterns of 2θ between 10° and 65°; (b) XRD patterns of 2θ between 20° and 35°.

of -15.33 mV due to the existing oxygen-containing functional groups, which is consistent with the result of UV-visible absorption and PL spectra of GQDs, while the pure ZnCdS shows a positive zeta potential of 14.39 mV. The modification of ZnCdS with GQDs causes a decrease in the zeta potential from 14.39 mV to 9.29 mV, indicating that the GQDs link together with ZnCdS by electrostatic attraction.

The crystal structure of the products was characterized by XRD analysis as shown in Figure 4. The main peaks of 2θ at 25.5°, 27.0°, 28.6°, 44.3°, 48.3°, and 52.4° can be assigned to the (100), (002), (101), (110), (103), and (112) crystal faces of hexagonal ZnCdS (JCPDS no. 89-2943), respectively. When GQDs are incorporated with ZnCdS, the diffraction peaks of ZnCdS present no obvious shift, which means that the introduction of GQDs has no effect on the lattice structure of the ZnCdS semiconductor. There are no characteristic peaks of GQDs observed in the GQDs-modified ZnCdS composites due to the low content and weak diffraction intensity of GQDs.

HRTEM was further applied to investigate the microstructures of the ZnCdS/G-0.06. The present lattice fringes of GQDs-modified ZnCdS composites can be assigned to GQDs and ZnCdS. As shown in Figure 5, the lattice spacing of 0.21 nm corresponds to the (100) plane of GQDs. The identified interplanar spacing of 0.175 nm corresponds to the (112) lattice plane of the ZnCdS phase which is in agreement with the result of XRD.

To further investigate the chemical states of ZnCdS/G-0.06, XPS analysis was performed. Figure 6 reveals the presence of Zn, Cd, S, and C in the composites. Zn 2p is divided to Zn $2p_{3/2}$ and Zn $2p_{1/2}$ that are located at bonding energies of 1021.4 eV and 1044.5 eV, respectively, while Cd 3d is divided to Cd $3d_{5/2}$ and Cd $3d_{3/2}$ located at

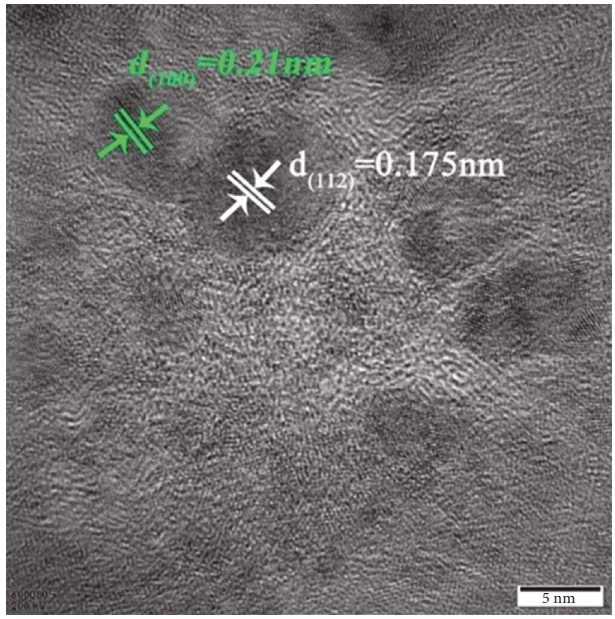

Figure 5: HRTEM image of ZnCdS/G-0.06.

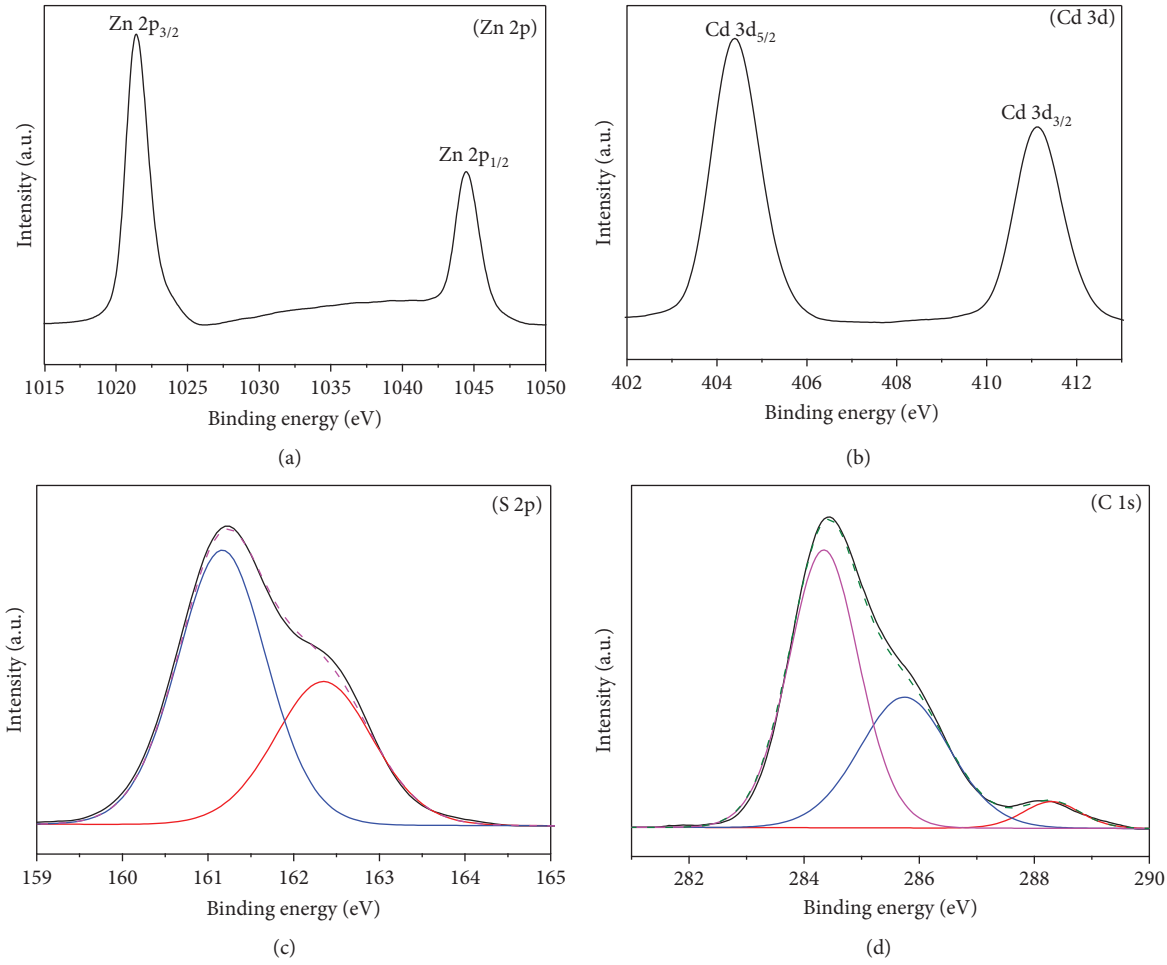

Figure 6: XPS spectra of ZnCdS/G-0.06: (a) Zn 2p XPS spectra; (b) Cd 3d XPS spectra; (c) S 2p XPS spectra; (d) C 1s XPS spectrum.

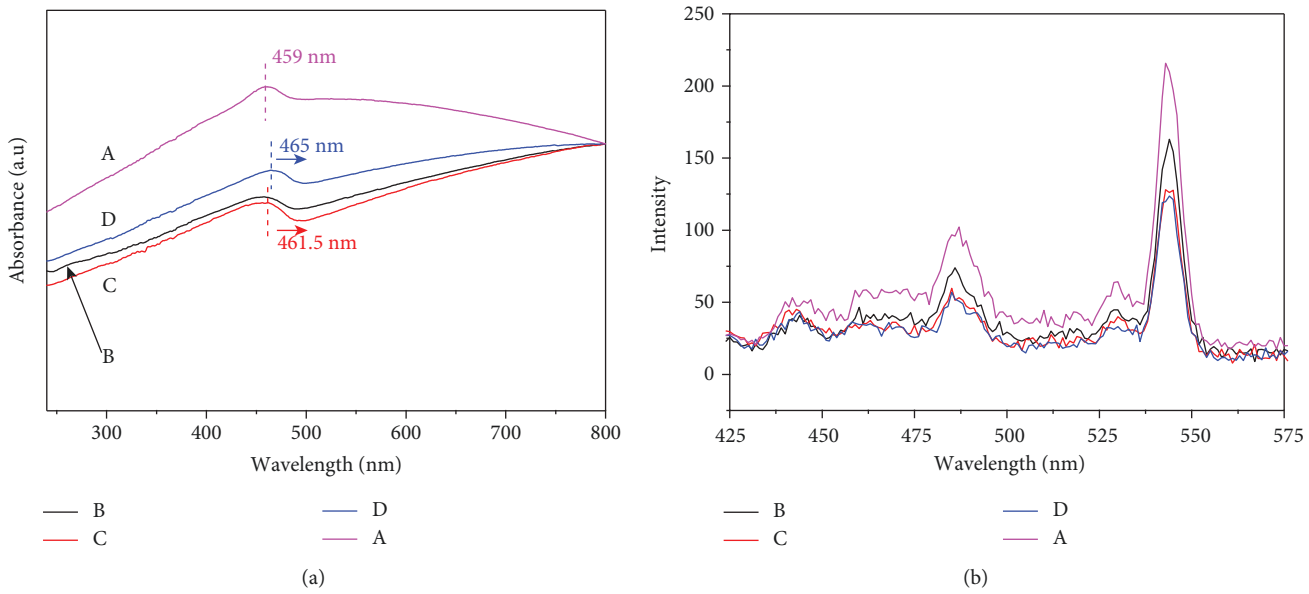

Figure 7: UV-visible absorption spectra and PL spectra of pure ZnCdS (A), ZnCdS/G-0.03 (B), ZnCdS/G-0.06 (C), and ZnCdS/G-0.12 (D).

around 404.4 eV and 411.1 eV, respectively. According to the literature data [9, 12], the binding energies of Zn 2p and Cd 3d are in line with Zn^{2+} and Cd^{2+}, indicating the fact that Zn and Cd exist in the form of Zn^{2+} and Cd^{2+} in the ZnCdS/G-0.06. The peak of S 2p is fitted with two peaks at approximately 161.2 eV and 162.4 eV. It indicates that sulphur exists in the form of S^{2-}. The detected C element originated from GQDs. The high-resolution spectrum of the C 1s region can be fitted by three main peaks, indicating the presence of carbon existing in three different chemical environments. The binding energy peak at 284.4 eV, 285.6 eV, and 288.3 eV corresponds to the sp2 C peak of C=C bonds, C-OH bond, and C=O bond, respectively.

The optical properties of all ZnCdS/G samples with different GQDs contents were characterized by the UV-visible absorption spectra and PL spectra. As shown in Figure 7(a), the UV-visible absorption spectra of pure ZnCdS show an efficient absorption edge to 459 nm, corresponding to the specific absorption peak of ZnCdS. Moreover, the absorption edges of ZnCdS/G composites had an obvious red shift with the increase of GQDs content. The significant red shift was due to the decrease of the bandgap energy when the GQDs were incorporated in ZnCdS crystals. The PL spectra were conducted under a 220 nm emission as shown in Figure 7(b). It reveals that the PL intensity decreases with the increase of the GQDs content. The decreased PL intensities of ZnCdS/G composites indicate that the GQDs facilitate the charge transfer and separation.

The effect of different GQDs additions on photoelectric properties was investigated by photocurrent-time responses. As shown in Figure 8, all the curves present an obvious anodic photocurrent spike at the initial time of irradiation, which resulted from the separation of the electron-hole pairs [40]. After that, the photocurrent intensity continuously decreases until it reaches stability, suggesting that recombination process occurs. When the light irradiation is off, the

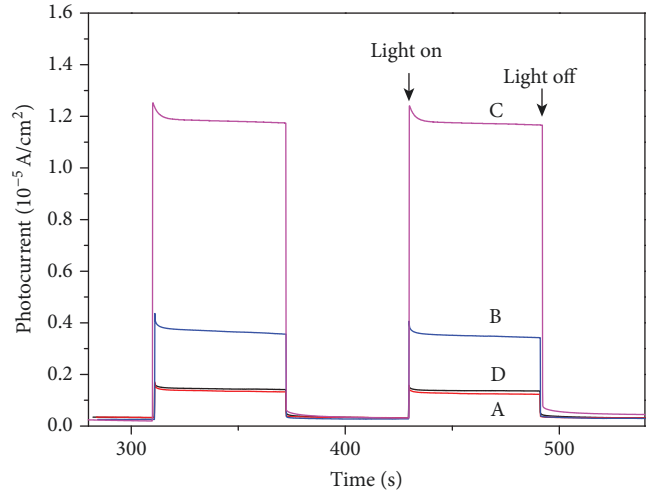

Figure 8: Photocurrent-time response of pure ZnCdS (A), ZnCdS/G-0.03 (B), ZnCdS/G-0.06 (C), and ZnCdS/G-0.12 (D).

charge carriers are released from the traps, resulting in the photocurrent decaying to zero [41]. Compared with the pure ZnCdS, the anodic photocurrent spikes of ZnCdS/G-0.06 are obvious, and the photocurrent intensity achieves a maximum of 11.4 μA/cm^2 which is 10 times as high as that of pure ZnCdS. The mechanism can be explained by Figure 9. It is not difficult to understand that the GQDs act as an influential role in the conductive channel of electrons, which can accelerate the separation efficiency of photo-generated electron-hole pairs and make it possible for more electrons to be transferred to the external circuit. It is clear that the photocurrent density decreases when the GQDs content increases to 0.12%, which is ascribed to the reason that superabundant GQDs particles are anchored on the ZnCdS particles resulting in a low light absorption efficiency. Figure 10

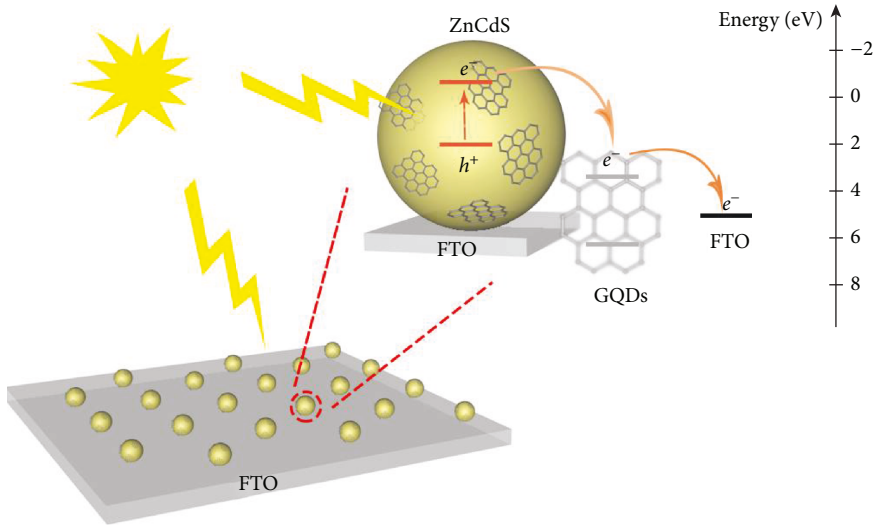

Figure 9: Schematic illustration of photo-generated electron transmission in ZnCdS/G composites.

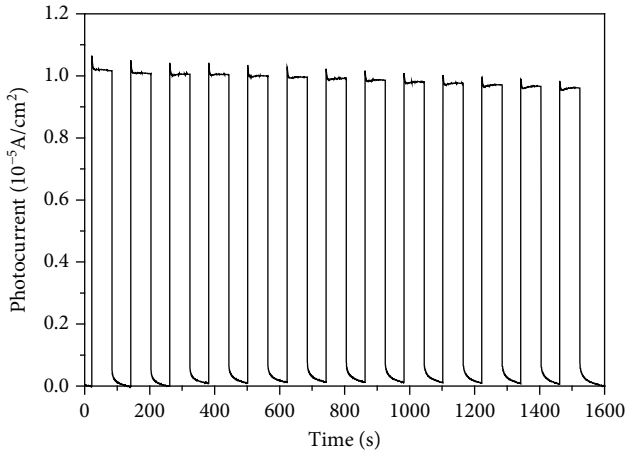

Figure 10: Photocurrent-time response of ZnCdS/G-0.06 at 1600 seconds.

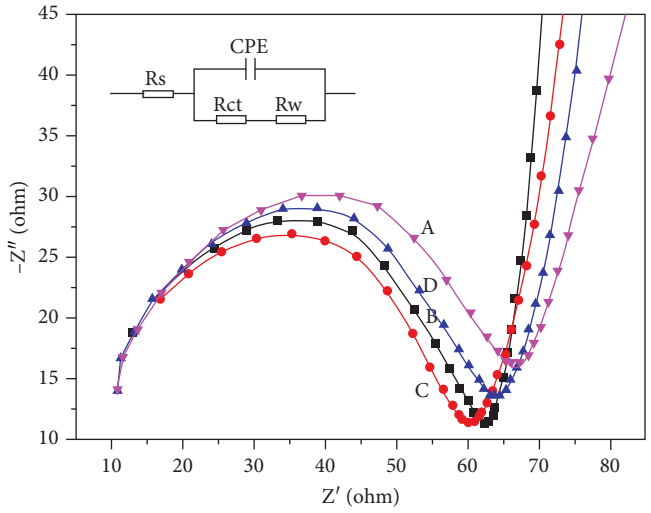

Figure 11: Electrochemical impedance spectra of pure ZnCdS (A), ZnCdS/G-0.03 (B), ZnCdS/G-0.06 (C), and ZnCdS/G-0.12 (D).

shows photocurrent counts as a function of time under intermittent illumination. The photocurrent density of ZnCdS/G-0.06 composites presents a decrease of 10% and remains stable after 1600 s.

To further study the role of GQDs in promoting electron transfer on the contact surfaces, electrochemical impedance was performed at an applied bias voltage of 500 mV. The Nyquist plots and an equivalent electrical circuit are shown in Figure 11. The Rs, Rw, and CPE denote the electrolyte resistance, Warburg impedance, and associated double-layer capacitance, respectively. The Rct denotes the charge transfer resistance corresponding to the semicircle in the high-frequency region [42]. As seen, the Rct value of pure ZnCdS is 56 Ω, while that of ZnCdS/G-0.06 decreases to 49 Ω. The apparent decreased Rct value for ZnCdS/G-0.06 shows a lower charge transfer resistance, which indicates that the presence of GQDs promotes electron transfer in the ZnCdS thin film. The result shows a minimum of electrochemical impedance at the addition of 0.06 wt% GQDs, which is consistent with the results of photocurrent-time response.

4. Conclusions

A series of different contents of GQDs-modified ZnCdS composites were successfully synthesized using the solvothermal route. With optimized GQDs decoration, the photoelectric and electrochemical performances of the composites have an obvious improvement to those of pure ZnCdS. The photocurrent density first increases and then decreases with the contents of GQDs changing from 0.03 wt% to 0.12 wt%. The composites at 0.06 wt% GQDs show a minimum of electrochemical impedance and achieve a maximum photocurrent value of 11.4 μA/cm^2 which is 10 times as high as that of pure ZnCdS. The enhanced photoelectric and

electrochemical performances can be attributed to the high conductivity of GQDs which not only accelerate the separation efficiency of photo-generated electron-hole pairs but also induce the reduction of the interfacial electronic resistance. Consequently, the present work offers a new insight into the fabrication of GQDs and ternary semiconductor composites for enhancing the semiconductor properties.

Data Availability

The data used to support the findings of this study are available from the corresponding author upon request.

Conflicts of Interest

The authors declare that there is no conflict of interest regarding the publication of this paper.

Acknowledgments

The work was supported by the National Natural Science Foundation of China (No. 51204129).

References

[1] V. M. Ramakrishnana, M. Natarajana, A. Santhanama, V. Asokanb, and D. Velauthapillaic, "Size controlled synthesis of TiO_2 nanoparticles by modified solvothermal method towards effective photo catalytic and photovoltaic applications," *Materials Research Bulletin*, vol. 97, pp. 351–360, 2018.

[2] M. Jourshabani, Z. Shariatinia, and A. Badiei, "Synthesis and characterization of novel Sm_2O_3/S-doped g-C_3N_4 nanocomposites with enhanced photocatalytic activities under visible light irradiation," *Applied Surface Science*, vol. 427, pp. 375–387, 2018.

[3] Y. C. Chen, C. B. Siao, H. S. Chen, K. W. Wang, and S. R. Chung, "The application of $Zn_{0.8}Cd_{0.2}S$ nanocrystals in white light emitting diodes devices," *RSC Advances*, vol. 5, no. 106, pp. 87667–87671, 2015.

[4] J. U. Zhang and F. X. Xiao, "Modulation of interfacial charge transfer by self-assembly of single-layer graphene enwrapped one-dimensional semiconductors toward photoredox catalysis," *Journal of Materials Chemistry A*, vol. 5, no. 45, pp. 23681–23693, 2017.

[5] X. C. Dai, M. H. Huang, Y. B. Li et al., "Regulating spatial charge transfer over intrinsically ultrathin-carbon-encapsulated photoanodes toward solar water splitting," *Journal of Materials Chemistry A*, vol. 7, no. 6, pp. 2741–2753, 2019.

[6] F. X. Xiao and B. Liu, "In situ etching-induced self-assembly of metal cluster decorated one-dimensional semiconductors for solar-powered water splitting: unraveling cooperative synergy by photoelectrochemical investigations," *Nanoscale*, vol. 9, no. 43, pp. 17118–17132, 2017.

[7] F. Zhang, C. L. Zhang, H. Y. Peng, H. P. Cong, and H. S. Qian, "Near-infrared photocatalytic upconversion nanoparticles/-TiO_2 nanofibers assembled in large scale by electrospinning," *Particle & Particle Systems Characterization*, vol. 33, no. 5, pp. 248–253, 2016.

[8] J. Y. T. Chan, S. Y. Ang, E. Y. Ye, M. Sullivan, J. Zhang, and M. Lin, "Heterogeneous photo-Fenton reaction on hematite (α-Fe_2O_3){104}, {113} and {001} surface facets," *Physical Chemistry Chemical Physics*, vol. 17, no. 38, pp. 25333–25341, 2015.

[9] C. C. Shen, Y. N. Liu, X. Zhou et al., "Large improvement of visible-light photocatalytic H_2-evolution based on cocatalyst-free $Zn_{0.5}Cd_{0.5}S$ synthesized through a two-step process," *Catalysis Science & Technology*, vol. 7, no. 4, pp. 961–967, 2017.

[10] M. Das, J. Datta, R. Jana, S. Sil, S. Halder, and P. P. Ray, "Synthesis of rGO-$Zn_{0.8}Cd_{0.2}S$ via in situ reduction of GO for the realization of a Schottky diode with low barrier height and highly enhanced photoresponsivity," *New Journal of Chemistry*, vol. 41, no. 13, pp. 5476–5486, 2017.

[11] D. H. Wang, L. Wang, and A. W. Xu, "Room-temperature synthesis of $Zn_{0.80}Cd_{0.20}S$ solid solution with a high visible-light photocatalytic activity for hydrogen evolution," *Nanoscale*, vol. 4, no. 6, pp. 2046–2053, 2012.

[12] S. N. Guo, Y. L. Min, J. C. Fan, and Q. J. Xu, "Stabilizing and improving solar H_2 generation from $Zn_{0.5}Cd_{0.5}S$ nanorods@-MoS_2/RGO hybrids via dual charge transfer pathway," *ACS Applied Materials & Interfaces*, vol. 8, no. 5, pp. 2928–2934, 2016.

[13] M. N. Huang, J. H. Yu, C. S. Deng et al., "3D nanospherical $Cd_xZn_{1-x}S$/reduced graphene oxide composites with superior photocatalytic activity and photocorrosion resistance," *Applied Surface Science*, vol. 365, pp. 227–239, 2016.

[14] O. Moradlou, N. Tedadi, A. Banazadeh, and N. Naseri, "Effect of RGO/$Zn_xCd_{1-x}S$ crystalline phase on solar photoactivation processes," *RSC Advances*, vol. 6, no. 52, pp. 46282–46290, 2016.

[15] E. Hong, D. Kim, and J. H. Kim, "Heterostructured metal sulfide (ZnS–CuS–CdS) photocatalyst for high electron utilization in hydrogen production from solar water splitting," *Journal of Industrial and Engineering Chemistry*, vol. 20, no. 5, pp. 3869–3874, 2014.

[16] W. N. Wang, C. X. Huang, C. Y. Zhang et al., "Controlled synthesis of upconverting nanoparticles/$Zn_xCd_{1-x}S$ yolk-shell nanoparticles for efficient photocatalysis driven by NIR light," *Applied Catalysis B: Environmental*, vol. 224, pp. 854–862, 2018.

[17] S. Ham, Y. Kim, M. J. Park, B. H. Hong, and D. J. Jang, "Graphene quantum dots-decorated ZnS nanobelts with highly efficient photocatalytic performances," *RSC Advances*, vol. 6, no. 29, pp. 24115–24120, 2016.

[18] H. S. Chen, S. R. Chung, T. Y. Chen, and K. W. Wang, "Correlation between surface state and band edge emission of white light $Zn_xCd_{1-x}S$ nanocrystals," *Journal of Materials Chemistry C*, vol. 2, no. 15, pp. 2664–2667, 2014.

[19] Y. C. Chen, H. S. Chen, S. R. Chung, J. K. Chang, and K. W. Wang, "The effect of surface structures and compositions on the quantum yields of highly effective $Zn_{0.8}Cd_{0.2}S$ nanocrystals," *Journal of Materials Chemistry C*, vol. 3, no. 23, pp. 5881–5884, 2015.

[20] J. M. Chen, J. Y. Chen, and Y. W. Li, "Hollow ZnCdS dodecahedral cages for highly efficient visible-light-driven hydrogen generation," *Journal of Materials Chemistry A*, vol. 5, no. 46, pp. 24116–24125, 2017.

[21] Y. L. Zhang, J. Cai, T. P. Ji et al., "Superionic conductor-mediated growth of ternary ZnCdS nanorods over a wide composition range," *Nano Research*, vol. 8, no. 2, pp. 584–591, 2015.

[22] K. H. Li, W. Liu, Y. Ni et al., "Technical synthesis and biomedical applications of graphene quantum dots," *Journal of Materials Chemistry B*, vol. 5, no. 25, pp. 4811–4826, 2017.

[23] S. H. Zhou, H. B. Xu, W. Gan, and Q. H. Yuan, "Graphene quantum dots: recent progress in preparation and fluorescence sensing applications," *RSC Advances*, vol. 6, no. 112, pp. 110775–110788, 2016.

[24] T. Fan, Y. L. Li, J. F. Shen, and M. X. Ye, "Novel GQDs-PVP-CdS composite with enhanced visible-light-driven photocatalytic properties," *Applied Surface Science*, vol. 367, pp. 518–527, 2016.

[25] K. Rahimi, A. Yazdani, and M. Ahmadirad, "Facile preparation of zinc oxide nanorods surrounded by graphene quantum dots both synthesized via separate pyrolysis procedures for photocatalyst application," *Materials Research Bulletin*, vol. 98, pp. 148–154, 2018.

[26] M. Managa, O. J. Achadu, and T. Nyokong, "Photophysical studies of graphene quantum dots - pyrene-derivatized porphyrins conjugates when encapsulated within Pluronic F127 micelles," *Dyes and Pigments*, vol. 148, pp. 405–416, 2018.

[27] B. Ahmed, S. Kumar, A. K. Ojha, F. Hirsch, S. Riese, and I. Fischer, "Facile synthesis and photophysics of graphene quantum dots," *Journal of Photochemistry and Photobiology A: Chemistry*, vol. 364, pp. 671–678, 2018.

[28] S. Samuei, J. Fakkar, Z. Rezvani, A. Shomali, and B. Habibi, "Synthesis and characterization of graphene quantum dots/-CoNiAl-layered double-hydroxide nanocomposite: application as a glucose sensor," *Analytical Biochemistry*, vol. 521, pp. 31–39, 2017.

[29] S. Kellici, J. Acord, N. P. Power et al., "Rapid synthesis of graphene quantum dots using a continuous hydrothermal flow synthesis approach," *RSC Advances*, vol. 7, no. 24, pp. 14716–14720, 2017.

[30] Z. P. Zeng, Y. B. Li, S. F. Chen, P. Chen, and F. X. Xiao, "Insight into the charge transport correlation in Au_x clusters and graphene quantum dots deposited on TiO_2 nanotubes for photoelectrochemical oxygen evolution," *Journal of Materials Chemistry A*, vol. 6, no. 24, pp. 11154–11162, 2018.

[31] Z. P. Zeng, T. Li, Y. B. Li et al., "Plasmon-induced photoelectrochemical water oxidation enabled by *in situ* layer-by-layer construction of cascade charge transfer channel in multilayered photoanode," *Journal of Materials Chemistry A*, vol. 6, no. 48, pp. 24686–24692, 2018.

[32] Z. P. Zeng, F. X. Xiao, H. Phan et al., "Unraveling the cooperative synergy of zero-dimensional graphene quantum dots and metal nanocrystals enabled by layer-by-layer assembly," *Journal of Materials Chemistry A*, vol. 6, no. 4, pp. 1700–1713, 2018.

[33] H. W. Tian, K. Shen, X. Y. Hu, L. Qiao, and W. T. Zheng, "N, S co-doped graphene quantum dots-graphene-TiO_2 nanotubes composite with enhanced photocatalytic activity," *Journal of Alloys and Compounds*, vol. 691, pp. 369–377, 2017.

[34] Y. G. Lei, C. Yang, J. H. Hou et al., "Strongly coupled CdS/graphene quantum dots nanohybrids for highly efficient photocatalytic hydrogen evolution: unraveling the essential roles of graphene quantum dots," *Applied Catalysis B: Environmental*, vol. 216, pp. 59–69, 2017.

[35] Y. Lei, F. F. Chen, and J. Xu, "Immobilizing ternary Zn_XCd1-_XS on graphene via solvothermal method for enhanced photoelectric properties," *Applied Surface Science*, vol. 357, pp. 155–159, 2015.

[36] Y. Lei, F. F. Chen, J. Xu, and Y. He, "Hydrothermal synthesis of ternary $Zn_XCd_{1-X}S$–graphene and its photoelectric properties," *Journal of Materials Science: Materials in Electronics*, vol. 26, no. 9, pp. 7200–7204, 2015.

[37] R. Z. Zhang, J. R. Adsetts, Y. T. Nie, X. H. Sun, and Z. F. Ding, "Electrochemiluminescence of nitrogen- and sulfur-doped graphene quantum dots," *Carbon*, vol. 129, pp. 45–53, 2018.

[38] S. J. Zhu, Y. B. Song, J. Wang et al., "Photoluminescence mechanism in graphene quantum dots: quantum confinement effect and surface/edge state," *Nano Today*, vol. 13, pp. 10–14, 2017.

[39] B. P. Qi, X. R. Zhang, B. B. Shang, D. S. Xiang, and S. H. Zhang, "Solvothermal tuning of photoluminescent graphene quantum dots: from preparation to photoluminescence mechanism," *Journal of Nanoparticle Research*, vol. 20, no. 2, pp. 1–9, 2018.

[40] Y. C. Yang, J. W. Wen, J. H. Wei, R. Xiong, J. Shi, and C. Pan, "Polypyrrole-decorated Ag-TiO_2 nanofibers exhibiting enhanced photocatalytic activity under visible-light illumination," *ACS Applied Materials & Interfaces*, vol. 5, no. 13, pp. 6201–6207, 2013.

[41] J. Zhang, J. G. Yu, M. Jaroniec, and J. R. Gong, "Noble metal-free reduced graphene oxide-$Zn_xCd_{1-x}S$ nanocomposite with enhanced solar photocatalytic H_2-production performance," *Nano Letters*, vol. 12, no. 9, pp. 4584–4589, 2012.

[42] J. W. Zhao, X. G. Kong, W. Y. Shi et al., "Self-assembly of layered double hydroxide nanosheets/Au nanoparticles ultrathin films for enzyme-free electrocatalysis of glucose," *Journal of Materials Chemistry*, vol. 21, no. 36, pp. 13926–13933, 2011.